COMPUTATIONAL DETAILS

The density functional theory (DFT) calculations and post-processing were performed using the QUANTUM ESPRESSO open-source software package [1]. The calculations utilized a plane-wave basis set with a kinetic energy cutoff of 350 eV, and projector augmented-wave pseudopotentials [2]. All relaxation calculations were performed with a force convergence threshold of 10^{-4} eV/Å. Experimental investigations of point defects in h-BN typically consider multi-layer samples, however, it has been shown that DFT calculations result in negligible differences between the electronic structure of defects in single- and multi-layer systems [3]. Our supercell consists of 98 atoms and a vacuum separation of 15 Å between layers, corresponding to 7×7 unit cells of mono-layer h-BN. The atomic positions and in-plane lattice constant for the pristine h-BN structure were relaxed using the Perdew-Burke-Ernzerhof (PBE) exchange-correlation functional [4]. An in-plane lattice constant of $a = 2.5$ Å was obtained, consistent with previous findings [5]. The Heyd-Scuseria-Ernzerhof (HSE06) hybrid functional [6] was then used to optimize the direct band-gap at the K high symmetry point [7] to the bulk value of ≈ 6 eV [8]. A band-gap of 5.98 eV was obtained by setting the mixing parameter to 0.32 and fine-tuning the screening parameter to 0.086/Å.

The C2Cn defect was then added to the hexagonal lattice, the atomic positions relaxed, and the ground state wavefunctions of the single particle defect levels were calculated. The symmetries of the wavefunctions in Fig. 1 allow for the determination of the relative energy orderings of the group theory orbitals. The b and b' orbitals have B_2 symmetry, i.e., anti-symmetric with respect to rotation about the diagonal in-plane axis. The a orbitals have A_2 symmetry, i.e., symmetric with respect to rotation about the diagonal in-plane axis. The energy ordering is $E_b < E_a < E_{b'}$.

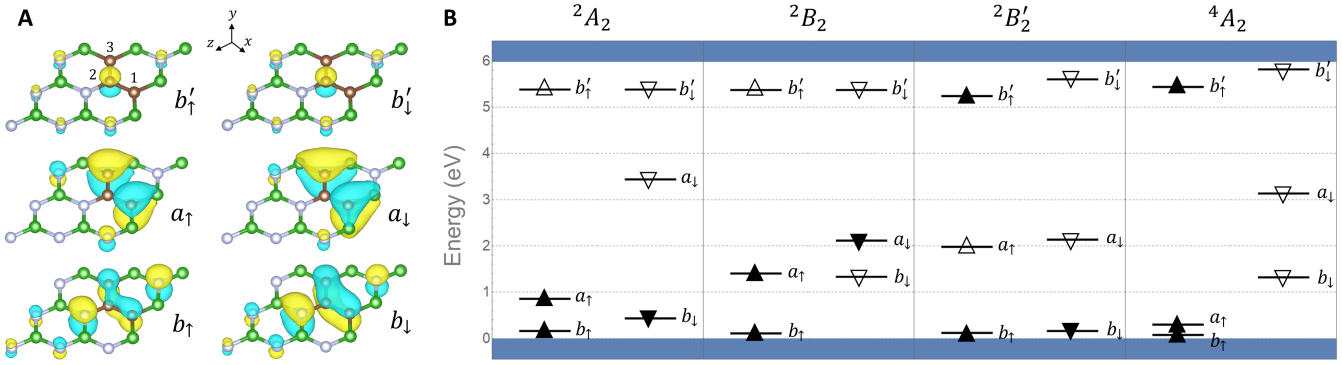

FIG. 1. (A) Ground state wavefunctions of the C2Cn defect. The positive (negative) components of each wavefunction are visualized by the yellow (blue) lobes. The corresponding symmetries are best represented when the b and a orbitals are plotted at an isosurface level of $\pm 0.007/\text{Å}^3$, and the b' orbitals at $\pm 0.0002/\text{Å}^3$.

Only the atoms and contributions to the wavefunction which are close to the carbon trimer defect are shown for simplicity. The carbon atoms are brown, boron atoms are green, and nitrogen atoms are grey. The diagrams were produced using VESTA [9]. (B) Defect levels of the ground state and single-configuration excited states in the fundamental band gap of h-BN. The occupied (unoccupied) levels are denoted by solid (empty) triangles.

Next, the single-configuration excited states ($^2A_2$, $^2B_2$, $^2B_2'$, and $^4A_2$) were created using the ΔSCF method [10], and the atomic positions of each excited state electronic configuration were relaxed. The transition energies between defect states were calculated by considering the difference in total energies of the structures, obtained via spin-polarized calculations performed within the Γ-point approximation. The HSE06 functional has been shown to provide accurate results for defects in h-BN which exhibit low correlation and charge transfer, and as such, it is expected that the error in the DFT calculations of the single-configuration states is on the order of 0.1 eV [11, 12]. The remaining states of interest ($^2A_2'$ and $^2A_2''$) are multi-configuration states which cannot be modelled in the DFT calculations using the ΔSCF method. Rough estimates for the corresponding transitions energies were obtained following the method of Ref. [13, 14], making use of the single-configuration states $|bab'\rangle$, $|ba\overline{b'}\rangle$, and $|b\overline{a}b'\rangle$ which were created within the ΔSCF procedure.

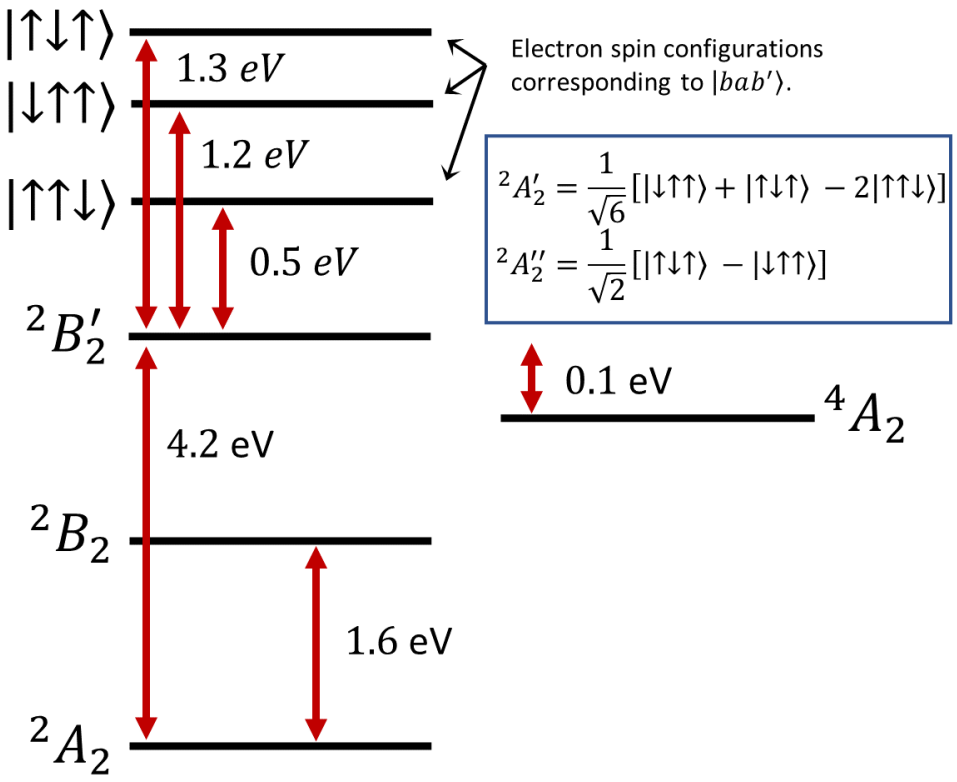

FIG. 2. Energy level diagram for the single-configuration multielectron states.

[1] P. Giannozzi, S. Baroni, N. Bonini, M. Calandra, R. Car, C. Cavazzoni, D. Ceresoli, G. L. Chiarotti, M. Cococcioni, I. Dabo, *et al.*, Journal of Physics: Condensed Matter **21**, 395502 (2009).
[2] P. E. Blöchl, Physical Review B **50**, 17953 (1994).
[3] T. T. Tran, K. Bray, M. J. Ford, M. Toth, and I. Aharonovich, Nature Nanotechnology **11**, 37 (2016).
[4] J. P. Perdew, K. Burke, and M. Ernzerhof, Physical Review Letters **77**, 3865 (1996).
[5] F. Ferreira, A. Chaves, N. Peres, and R. Ribeiro, JOSA B **36**, 674 (2019).
[6] J. Heyd, G. E. Scuseria, and M. Ernzerhof, The Journal of Chemical Physics **118**, 8207 (2003).
[7] D. Wickramaratne, L. Weston, and C. G. Van de Walle, The Journal of Physical Chemistry C **122**, 25524 (2018).
[8] M. Abdi, J.-P. Chou, A. Gali, and M. B. Plenio, ACS Photonics **5**, 1967 (2018).
[9] K. Momma and F. Izumi, Journal of Applied Crystallography **44**, 1272 (2011).
[10] A. Gali, E. Janzén, P. Deák, G. Kresse, and E. Kaxiras, Physical Review Letters **103**, 186404 (2009).
[11] J. R. Reimers, A. Sajid, R. Kobayashi, and M. J. Ford, Journal of Chemical Theory and Computation **14**, 1602 (2018).
[12] C. Jara, T. Rauch, S. Botti, M. A. Marques, A. Norambuena, R. Coto, J. Castellanos-Águila, J. R. Maze, and F. Munoz, The Journal of Physical Chemistry A **125**, 1325 (2021).
[13] D. H. Ess, E. R. Johnson, X. Hu, and W. Yang, The Journal of Physical Chemistry A **115**, 76 (2011).
[14] M. Mackoit-Sinkevičienė, M. Maciaszek, C. G. Van de Walle, and A. Alkauskas, Applied Physics Letters **115**, 212101 (2019).